DTIC FILE COPY

SECURITY CLASSIFICATION OF THIS PAGE

REPORT DOCUMENTATION PAGE

1a

1b RESTRICTIVE MARKINGS

2a

2b AD-A222 004

3. DISTRIBUTION / AVAILABILITY OF REPORT

APPROVED

4. Technical Report No. 14

5. MONITORING ORGANIZATION REPORT NUMBER(S)

6a. NAME OF PERFORMING ORGANIZATION: IBM Research Division

6b. OFFICE SYMBOL (If applicable)

7a. NAME OF MONITORING ORGANIZATION: ONR

6c. ADDRESS (City, State, and ZIP Code): P. O. Box 218, Yorktown Heights, NY 10598

7b. ADDRESS (City, State, and ZIP Code): Department of Navy, Arlington, VA 22217

8a. NAME OF FUNDING / SPONSORING ORGANIZATION: ONR

8b. OFFICE SYMBOL (If applicable)

9. PROCUREMENT INSTRUMENT IDENTIFICATION NUMBER: Contract N 00014-87-C-0701, Mod. #P0003

8c. ADDRESS (City, State, and ZIP Code): Chemistry Program Office, Arlington, VA 22217

10 SOURCE OF FUNDING NUMBERS

PROGRAM ELEMENT NO.	PROJECT NO.	TASK NO.	WORK UNIT ACCESSION NO

11. TITLE (Include Security Classification): Surface Photovoltage on Si(111)-(7X7) Probed by Optically-Pumped Scanning Tunneling Microscopy

12. PERSONAL AUTHOR(S): R.J. Hamers and K. Markert

13a. TYPE OF REPORT: Technical

13b. TIME COVERED: FROM _____ TO _____

14. DATE OF REPORT (Year, Month, Day): May 25, 1990

15. PAGE COUNT

16. SUPPLEMENTARY NOTATION

17. COSATI CODES

FIELD	GROUP	SUB-GROUP

18. SUBJECT TERMS (Continue on reverse if necessary and identify by block number): Photovoltage, Silicon, STM

19. ABSTRACT

Scanning Tunneling Microscopy is combined with optical excitation techniques to probe spatially-resolved, non-equilibrium electronic transport processes at the Si(111)-(7X7) surface. Photo-excited carriers separate in the sub-surface space-charge region, producing a surface photovoltage which is detected using the STM tip as a potentiometer. While the photovoltage is uniform on well-ordered regions of Si(111)-(7X7), strong decreases are observed near virtually all defects. Differences in the functional dependence of the photovoltage on the illumination intensity are also observed. The spatial dependence of the photovoltage primarily results from spatial variations in the local surface recombination rate.

DTIC ELECTE MAY 30 1990 S D

20. DISTRIBUTION / AVAILABILITY OF ABSTRACT: ☒ UNCLASSIFIED/UNLIMITED ☐ SAME AS RPT ☐ DTIC USERS

21. ABSTRACT SECURITY CLASSIFICATION: Unclassified

22a NAME OF RESPONSIBLE INDIVIDUAL: Dr. Mark Ross

22b TELEPHONE (Include Area Code): (202) 696-4410

22c. OFFICE SYMBOL

DD FORM 1473, 84 MAR — 83 APR edition may be used until exhausted. All other editions are obsolete.

SECURITY CLASSIFICATION OF THIS PAGE

90 05 25 023

OFFICE OF NAVAL RESEARCH

CONTRACT N00014-87-C0701

R&T Code 413F002

Technical Report No. 14

Surface Photovoltage on Si(111)-(7X7) Probed by Optically-Pumped Scanning Tunneling Microscopy

by

R.J. Hamers and K. Markert

Prepared for Pulication

in

Journal of Vacuum Science and Technology A

IBM Research Division
T.J. Watson Research Center
Yorktown Heights, N.Y. 10598

May 15, 1990

Reproduction in whole or in part is permitted for any purpose of the United States Government

This document has been approved for public release and sale; its distribution is unlimited

SURFACE PHOTOVOLTAGE ON Si(111)-(7X7) PROBED BY OPTICALLY-PUMPED SCANNING TUNNELING MICROSCOPY

R.J. Hamers and K. Markert

IBM T.J. Watson Research Center, Yorktown Heights, N.Y. 10598

Scanning Tunneling Microscopy is combined with optical excitation techniques to probe spatially-resolved, non-equilibrium electronic transport processes at the Si(111)-(7X7) surface. Photo-excited carriers separate in the sub-surface space-charge region, producing a surface photovoltage which is detected using the STM tip as a potentiometer. While the photovoltage is uniform on well-ordered regions of Si(111)-(7X7), strong decreases are observed near virtually all defects. Differences in the functional dependence of the photovoltage on the illumination intensity are also observed. The spatial dependence of the photovoltage primarily results from spatial variations in the local surface recombination rate.

Accession For
NTIS GRA&I ☒
DTIC TAB ☐
Unannounced ☐
Justification
By
Distribution/
Availability Codes
Dist | Avail and/or Special
A-1

DTIC COPY INSPECTED

I) Introduction

Since its invention in the early 1980's, the scanning tunneling microscope has proven itself as a versatile tool capable of addressing questions in a wide variety of areas. An increasing number of studies have used STM to explore the *electronic* properties of surfaces on an atomic scale, through measurements of the I-V characteristics. While tunneling I-V curves provide useful information about the *equilibrium* electronic state density of the surface, in many applications dynamic phenomena such as carrier transport and recombination [1-4] are of primary importance. Most carrier dynamics occurs on time scales far faster than what can be recorded with conventional STM electronics. However, information on fast non-equilibrium processes can often be obtained by driving the system away from its equilibrium state and studying the steady-state (but non-equilibrium) response.

In this paper, we report on recent investigations combining optical excitation with scanning tunneling microscopy to probe the non-equilibrium electronic properties of silicon surfaces. [5] Unlike previous studies, which have studied the thermal expansion of the sample and tip as a result of optical absorption [6] we directly probe the non-equilibrium changes in the distribution of charge carriers produced by optical excitation. This is accomplished by utilizing the surface photovoltage (SPV) effect. [7-11] As a result of high density of mid-gap surface states on silicon surfaces, charge transfer between surface and bulk states occurs, with the concurrent formation of a sub-surface space-charge layer. The electric field in this space-charge layer changes the potential energy of the electrons, so that the energies of the valence and conduction bands change between the bulk and the surface, a phenomenon usually referred to as "band-bending". On silicon surfaces, the band-bending is such that at the surface, the Fermi level lies midway between the valence and conduction band edges, irrespective of the bulk doping

of the material.[12, 13] As a consequence, the band-bending is downward on p-type samples and upward on n-type samples.

As illustrated in figure 1, illumination of this surface with light having energy greater than the bulk bandgap will excite electrons from the valence to the conduction band, thereby creating a bulk electron-hole pair. Since the absorption depth[14] of light at 488 nm is $\simeq 10^6$ Å, electron-hole pairs are created not only near the surface, but also comparatively deep into the bulk of the sample. In most of the bulk there is no electric field, so that the concentration of electrons is the same as the concentration of holes. In the space-charge region, however, the electric field separates the electron-hole pairs. On p-type samples (with downward band-bending), the electric field drives the electrons toward the surface and the holes into the bulk, while just the opposite occurs on n-type samples. As a result, there will be a non-equilibrium accumulation of electrons at the surface of a p-type sample, and a depletion of electrons at the surface of an n-type samples. The accumulation of carriers of one charge and the depletion of those of the other charge in the near-surface region generates a voltage, referred to as the "Surface Photovoltage", or SPV.

In the "optical pumping" scheme, the carrier transport can be viewed as a circulation, consisting of three steps: 1) Excitation, 2) Drift in the sub-surface space charge region, 3) Recombination mediated by surface states. For a fixed excitation rate, the steady-state SPV is essentially a competition between drift in the electric field (which is determined by the magnitude of the band-bending) and the surface recombination. In our experiments, we probe the magnitude and sign of the SPV using the STM tip as a potentiometer.

II) Experimental:

All experiments were conducted under ultrahigh vacuum conditions, using a small lever-approach STM. The approach mechanism is similar in concept to that reported earlier, except that the present microscope is smaller by a factor of two. The X,Y scanner is made from from a thin square sheet of piezoelectric material by removing four triangular sections, to leave behind an X-shape scanner with an attached mounting frame. The Z-piezo is a short tube placed in back of the X-Y scanner.

Samples are prepared in a analysis/preparation chamber equipped with Low-energy Electron Diffraction, Auger Electron Spectroscopy, and a quadrupole mass spectrometer, with a base pressure of $8X10^{-11}$ Torr. After carefully degassing at $\simeq$ 1000 K for at least 12 hours, the samples are annealed at 1400 K for approximately 30 seconds, and cooled over 3-5 minutes. After approximately 30 minutes, they are transferred to a second, connected chamber containing the STM.

In order to observe the effect of bulk doping on our observations, samples with several bulk dopings were utilized. N-type samples with resistivities of 0.1 ohm-cm and 0.005 ohm-cm, and P-type samples with resistivities of 0.1 ohm-cm and 0.006 ohm-cm were used. Equivalent results were obtained on both n-type and p-type samples, except that the sign of the SPV is opposite due to the different directions of the band-bending. All results shown here were made on p-type samples.

Optical illumination was provided by a 10 mW He-Ne laser at 632.8 nm, or a multiline argon-ion laser operating at 488-514 nm with a maximum power of 100 mW. As depicted in Figure 2, the linearly-polarized laser light passes through an electro-optic modulator (EOM) and a polarizing prism (PP), to allow the laser intensity at the tip to be varied under computer control. A fraction of the beam is split off and measured using a silicon photodiode (PD), while the remainder of the laser reflects off two steering mirrors, passes through the window

of the vacuum system, and strikes a 1-inch focal length lens mounted directly on the STM. The tip is located approximately 90% of the way between the lens of its focal point, in order to illuminate a conveniently large area of the sample. Approximately 0.5 millimeter of the tip is also illuminated. The light approaches the tunnel junction at glancing incidence (nearly parallel to the surface plane) with its electric field vector parallel to the tip (P-polarization).

One significant effect produced by the optical excitation is that absorption of light by either sample or tip will lead to a small temperature increase, which in turn will cause a thermal expansion and a decrease in the width of the tunneling gap, as discussed previously.[6] In general, our experiments are conducted under conditions where the system is at thermal equilibrium in the presence of the optical excitation. Although thermal expansions of more than 10,000 Å can be produced if the light is inadvertently focussed on the shank of the tip, we find that when the light is properly focussed in the tunnel junction region the thermal expansion is typically between 20 and 100 Å when the laser is turned on. As discussed later, measuring this thermal expansion allows us to place an upper bound on the temperature rise of the sample due to the optical absorption.

III) Results and Discussion

a) Local Surface Photovoltage Measurement

The surface photovoltage (SPV) effect can be observed in several ways. Figure 3 shows two tunneling I-V curves measured on a Si(111)-(7X7) surface, one with illumination and the other without. In the absence of illumination, zero applied voltage always results in zero tunneling current. When illuminated, however, a photoelectric current is observed even with zero applied bias, and the resulting I-V curve crosses the x-axis at a non-zero voltage. The voltage which

must be applied to the sample in order to make the current equal to zero is equal in magnitude (but opposite in sign) to the surface photovoltage.

While it is possible to measure the surface photovoltage as a function of position by recording these tunneling I-V curves at each location, it is possible to obtain the same information in a more efficient manner by using the STM tip as a potentiometer. As shown in figure 4, DC potentiometry is performed by dividing the feedback cycle into two short time intervals of $\simeq$500 microseconds each. During the first half of the cycle, a constant bias voltage is applied to the sample; sample-and-hold circuit SH1 is in "sample" mode, so that the amplified tunneling current signal passes into the feedback controller FB1, which applies a voltage to the Z-piezo to maintain constant tunneling current. This part of the cycle is functionally equivalent to measuring the conventional STM "topography".

During the second part of the cycle, the feedback controller FB1 is disabled by placing SH1 in "hold" mode, and a *second* feedback controller FB2 is activated. This controller compares the actual tunneling current with zero, and applies a voltage to the sample bulk in order to maintain zero tunneling current. For an unilluminated sample, the Fermi level is constant throughout the sample, so this voltage will be zero. On an illuminated sample, however, this voltage will correspond to the potential difference between the bulk and the surface of the sample. This part of the feedback cycle is a DC potentiometry measurement. The advantage of such a DC potentiometry measurement is that since the SPV measurements are made under conditions of zero tunneling current, they are (to a first approximation) independent of the local tunneling probability as well as the sample-tip separation.

Figure 5 shows some results obtained on Si(111)-(7X7) using this DC potentiometry system. The upper left panel (fig. 5a) shows the topographic image, obtained during the first half of the feedback cycle with a voltage of -1.0 V

applied to the sample during the first part of the feedback cycle. The adatoms of the (7X7) reconstruction are clearly resolved, as is the asymmetry between the faulted and unfaulted halves of the unit cell. Several types of defects are also observed. Slightly left of the center of the image is a boundary between two different (7X7) domains; this extended line defect is decorated with a higher degree of disorder as the adatoms attempt to maintain optimal coordination at the boundary. Additionally, several types of other defects can be observed, some of which appear as protrusions and some as depressions. The lower left panel, figure 5b, shows the spatial dependence of the surface photovoltage, obtained simultaneously with the topographic image shown in fig. 5a. In regions where the topographic image shows a well-ordered (7X7) reconstruction, the average photovoltage is -180 mV, corresponding to an accumulation of electrons at the surface. At locations where the topographic image shows disordered adatoms or other types of defects, the photovoltage image shows a substantial decrease; at small defects, it decreases to less than half this value, while at large defects (such as in the upper left corner of the image), it drops to essentially zero. It should be noted that statistics accumulated from many such images show that more than 95% of atomic-sized defects decrease the local photovoltage, irrespective of whether the defects appear as protrusions or depressions in the topography and irrespective of whether the doping in n-type or p-type.

On the ordered (7X7) surface, we find that the the photovoltage is always opposite in sign on p-type and n-type samples, corresponding to surface accumulations of photo-electrons at the surface on p-type samples, and photo-holes on n-type samples. This is a direct result of the mid-gap pinning of the surface Fermi level position by the adatom surface state of the (7X7) reconstruction. A potentially important application of these photovoltage measurements is that measuring the sign of the surface photovoltage can be used to directly *determine* the doping in the near-surface region with extremely high spatial resolution. The

spatial resolution observed here at defects is typically 20-30 Å. The length scale of the SPV will be discussed in more detail later, but appears to be determined by the bulk electrostatic screening length (here, $\simeq$ 80 Å) which is reduced in the near-surface region by the high density of surface states.

Figures 5c and 5d show this same data as three-dimensional representation, which more clearly shows some aspects of the experimental results. Here, the three-dimensional height is keyed to the actual height of the sample, while the brightness at each location is keyed to the local curvature. In the three-dimensional view, it can be observed that the "atomic-resolution" modulation in the SPV is $\simeq$ 10% of the total SPV, while at the defects much larger decreases in the SPV signal are observed; these can also be observed in the top-view images.

Toward the end of the acquiring figure 5, the laser was blocked. In the topographic image (5c), it can be seen that blocking the laser causes a sudden drop in the apparent height of the surface. This is a photothermal effect, arising from the small temperature increase (primarily of the tip) induced by optical illumination, which quickly recovers when illumination stops. The sudden height change here corresponds to a contraction of $\simeq$ 35 Å, followed by a slower continued drift. A careful look in this latter part of the image shows that atomic resolution is still maintained after blocking the laser, as three "corner holes" of the (7X7) reconstruction are still visible. The corresponding photovoltage image (5d) shows that blocking the laser completely eliminates the SPV signal, leaving only a small amount of residual noise. This 3-dimensional view shows two important characteristics of the residual noise. First, the noise is much smaller than the corrugations in the SPV observed with illumination, demonstrating that even the "atomic-scale" corrugation in the SPV is a real effect. Secondly, in the absence of illumination, there is no correlation between the "noise" and the sample topography (which is still visible on the declining portion of fig. 5c). This demonstrates that the SPV signal is derived *entirely* from the non-equilibrium electronic

state populations induced by the optical excitation. We further note that the absence of any difference between the surface and bulk potentials when the laser is blocked demonstrates that the application of V_{stab} does not produce any significant population of long-lived "trap" states. Thus, on these surfaces all changes in surface charge are completed on time scales which are short compared to the feedback cycle time of approximately 500 microseconds.

In addition to the photovoltaic effect illumination of the silicon surface also leads to a temperature increase, with a concurrent *thermo*electric voltage. The magnitude of such thermoelectric voltages can be estimated in two ways. First, numerical calculations based on the illumination intensity [15] predict that under the conditions used here, the temperature rise induced by optical excitation is approximately 3 Kelvin at the surface, decreasing into the bulk. Since the thermoelectric coefficient[14] of P-type, 0.1 ohm-cm silicon is 1 mV/Kelvin, this corresponds to 3 millivolts of thermoelectric potential, which is negligible compared to the surface photovoltage we observe.

An upper bound on the surface temperature rise can also be obtained directly from the STM results, by measuring the change in apparent surface height when the laser is blocked. Since the diameter of the laser beam at the sample is larger than the sample thickness of 0.35 mm, the front and back surfaces of the sample will be at nearly the same temperature. Under these conditions, the photothermal expansion Δh is approximately: [16] $\Delta h = \alpha \Delta T L$, where α is the thermal expansion coefficient ($2.6 \times 10^{6}\ K^{-1}$), L is the sample thickness, and ΔT is the temperature increase induced by optical absorption. In figure 5 we observed a change in apparent height of $\simeq$35Å when the laser was blocked. Although we believe that most of this arises from the expansion of the tip, we shall assume that all the expansion arises from the sample. Then, $\Delta h = 35$Å, from which we estimate $\Delta T = 4$ Kelvin, again indicating that that maximum thermoelectric potential will be approximately 4 millivolts. Although the com-

plicated sample-tip geometry makes accurate determination impossible, it is clear from both these calculations that at the power levels used here temperature rises are small and thermoelectric voltages are negligible compared to the surface photovoltage.

From figure 5, and by statistical analysis of a large number of such images, we find that more than 95% of all defects strongly decrease the photovoltage over distances of $\simeq$ 20Å, both on n-type and p-type samples. To understand the origin of the decreased SPV near defects, we note that the observed photovoltage is a steady-state voltage determined both by the rate at which carriers drift toward the surface (which is determined in turn by the band-bending) and the rate at which the electron-hole pairs recombine at the surface. As a result, the observation of a reduced photovoltage can have two main origins. First, it could arise from a surface location where the band-bending is small, so that the electric field in the subsurface space-charge region is small. Second, it could arise from a region of the surface which allows the electrons and holes to recombine.

b) Intensity dependence of SPV

It is possible to distinguish between these processes from measurements of the photovoltage as a function of laser intensity. Previous studies of surface recombination in macroscopic samples have shown that in the low-injection limit (i.e., low laser intensities), the photovoltage can be expressed as: $V_{SPV} = A \log(1 + \frac{\delta n + \delta p}{n + p})$, where the constant A is kT/q (= 26 mV), δn and δp are the densities of photoexcited electrons and holes, and n and p are the total densities of electrons and holes. The density of photoexcited electrons and holes is proportional to the laser intensity I, so that the functional dependence of the SPV on the illumination intensity can be rewritten as: $V = A \log(1 + BI)$, where the constant B is inversely proportional to the surface recombination velocity. In

our experiments we do not know the exact illumination intensity I due to possible shadowing and diffraction by the tip; however, the intensity I will always be proportional to the laser power P, so that this expression can be rewritten as $V = A \log(1 + B'P)$. In order to investigate whether this simple formula is appropriate, we made measurements of the photovoltage as a function of laser intensity. In these measurements, the electro-optic modulator was used to control the laser intensity, while the computer recorded both the actual laser intensity as well as the observed photovoltage. As the intensity is increased, there is a small photothermal expansion of sample and tip; by ramping the laser power slowly (2 Hz), the STM "topography" feedback loop completely corrected for this expansion, thereby maintaining a constant sample-tip separation even as the laser intensity was changed.

Figure 6 shows experimental results obtained on a Si(111)-(7x7) sample, using approximately 30 seconds of signal averaging. Also shown is a two-parameter fit to the log function $V = A \log(1 + B'P)$, using $A = 30.6$ mV and $B = .40$ Watts^{-1}. Clearly, we find excellent agreement between our experimental functional dependence and that predicted from the above theory, over more than three orders of magnitude in laser intensity. Additionally, we note that the the value of $A = 30.6$ mV obtained from the fit is in reasonable agreement with the expected value of 26. mV at 300 Kelvin. We believe the slight difference results from small systematic errors in the calibration of our apparatus. We also rule out any possiblity of a significant temperature rise, since if the sample temperature increased as a result of the illumination, it should equilibrate within the half-second duration of the intensity ramp; as a result, a significant illumination-induced temperature change would produce a deviation from logarithmic behavior, which we do not observe. We are unable to make a direct comparison of the value of B with theory, except to note that this value indicates that at the

highest intensity the optical illumination increases the steady-state minority carrier density by a factor of 40, which seems quite reasonable.

In order to understand the origin of the large decreases in the SPV signal observed near defects, we also obtained such measurements on defects of nanometer dimensions. In these experiments, the laser was held at a fixed intensity during most of the raster-scan. At selected locations the raster-scanning was stopped, and a laser intensity was ramped in a linear fashion while simultaneously recording the photovoltage. After averaging several of these curves together to improve the statistics, the laser was returned to its initial value and the raster-scanning was continued. Such spatially-localized measurements were made at several locations in order to be able to compare the functional dependence of the SPV on intensity at the different locations within a single STM image.

Figure 7a shows an STM scan of a small surface area including a defect induced by exposure to $\simeq$ 100 Langmuirs oxygen, and figure 7b shows the corresponding SPV image. At the locations denoted by the arrows, measurements of the SPV as a function of intensity were made, as shown in figure 7c. Clearly, the curves obtained on the (7X7) region and at the defect are quite different. On the Si(111)-(7X7) region, the SPV varies according to $V = A \log(1 + BI)$ at low intensities, but at higher intensities a saturation of the SPV is evident. This is in stark contrast to the behavior observed at the defect; here, the SPV is generally much lower, and, more importantly, shows no sign of saturating as the illumination intensity is increased further. A fit of the observed curve to the log function at low intensity indicates a surface recombination velocity roughly 5 times higher than on the ordered (7x7) region. The observation that the defect shows only a small SPV which does not saturate with increased intensity is only consistent with the conclusion that the defect acts as an efficient recombination center for electron-hole pairs.

One of the rather unique features of the clean Si(111)-(7X7) surface is that the density of surface states is essentially continuous between the valence and conduction band edges. Both STM[17] as well as photoemission spectroscopy[18] show that the (7X7) surface is very metallic. In general, such a metallic surface would be expected to give rise to a high recombination rate, since electrons in the conduction band can easily cascade down through the surface states back into the valence band. Recombination mediated by a metallic surface is therefore expected to be very efficient, as multiphonon processes are not required. Yet, this simple model appears to require modification. Our results show that defects induced by sub-monolayer oxidation, which *reduce* the density of states within the gap, actually lead to an *increase* in the recombination rate. We believe this apparent contradiction can be adequately explained by a more detailed consideration of the nature of the surface states and their role in the recombination process.

In previous tunneling spectroscopy measurements, Hamers, et al. [17] showed that on Si(111)-(7X7), the surface state nearest the Fermi level arises from the twelve adatoms within the unit cell, and is also fairly sensistive to the long-range order. Similarly, ultraviolet photoemission measurements often see that this adatom state is strongly affected by even trace amounts of contamination. This indicates that this state is intimately connected with the long-range, two-dimensional order of the surface. In that sense, it is essentially a two-dimensional Tamm state.

The photoexcited carriers, on the other hand, are primarily in the three-dimensional bulk conduction band. For recombination to take place via the surface states, the electron must somehow get from the three-dimensional conduction band into this two-dimensional surface state. Since the carriers drifting in the electric field of the space-charge region have significant momentum perpendicular to the surface plane, they must undergo an inelastic scattering process in order

to eliminate their perpendicular momentum before they can relax into the two-dimensional surface states. Our results indicate that the primary role of surface defects may be to locally destroy the two-dimensional nature of the surface states, thereby providing a way of scattering electrons from the three-dimensional bulk states into the two-dimensional surface states. This also indicates that momentum conservation, rather than energy conservation, may be the rate-limiting factor in the scattering of electrons from conduction to surface states.

c) Spatial resolution: Nanometer and Atomic-scale SPV variations

We consider here the spatial extent of the observed SPV features. Under conditions of steady-state illumination, we expect the SPV to have a spatial extent corresponding to some kind of electrostatic screening length. Although the screening length is well-defined in the bulk of an ideal semiconductor (the Debye length, here $\simeq$ 80 Å), the electrostatics at the surface is somewhat more complicated. In general, dopant segregation increases the dopant concentration in the near-surface regions, decreasing the electrostatic screening length. For any semiconductor with surface states within the bulk gap, however, the surface states themselves will tend to reduce the screening length. In particular, the Si(111)-(7X7) surface has a very high density of electrons close to the Fermi level, so that small changes in the local potential can be screened by only small changes in the surface state populations. Thus, mid-gap surface states further decrease the effective screening length at the surface, by an amount which depends both on the density of surface states near E_F and the two-dimensional electrical conductivity in the surface states. Accurate prediction of the effective surface screening length then requires solving Poisson's equation in three dimensions explicitly including the density and conductivity of the surface states. Although we do not include such calculations here, it is clear that the high density of sur-

face states produces a further decrease in the screening length and the possibility of increased spatial resolution.

IV) Conclusions

By combining STM with optical excitation, it is possible to probe *non*-equilibrium electronic properties of surfaces with extremely high spatial resolution. The surface photovoltage effect allows us to probe the non-equilibrium carrier distributions created by optical excitation of semiconductors, with very high spatial resolution. The information obtained with this combination provides new insight into the role of surface states and surface imperfections in carrier transport and recombination processes.

V) Acknowledgments

The authors wish to gratefully acknowledge the financial assistance of the U.S. Office of Naval Research as well as fruitful discussions with Joachim Clabes and Joe Demuth.

[1] W. Shockley and W.T. Read, Phys. Rev. **87**, 835 (1952).

[2] R.N. Hall, Phys. Rev. **83**, 228 (1951).

[3] W.H. Brattain and J. Bardeen, Bell Sys. Tech. J. **32**, 1 (1953.).

[4] D.T. Stevenson and R.J. Keyes, Physica **20**, 1041 (1954).

[5] R.J. Hamers and K.W. Markert, Phys. Rev. Lett. **64**, 1051 (1990).

[6] Amer, N. M., Skumanich, A., and Ripple, D., Appl. Phys. Lett. **49**, 137 (1986).

[7] J. Lagowski, C.L. Balestra, and H.C. Gatos, Surf. Sci. **29**, 213 (1972).

[8] W.Kuhlmann and M. Henzler, Surf. Sci. **99**, 45 (1980).

[9] J. Clabes and M. Henzler, Phys. Rev. B **21**, 625 (1980).

[10] L.J. Brillson and D.W. Kruger, Surf. Sci. **102**, 518 (1981).

[11] W. Mönch, P. Koke, and S. Krüger, J. Vac. Sci. Technol. **19**, 313 (1981).

[12] F.G. Allen and G.W. Gobeli, Phys. Rev. **127**, 150 (1962).

[13] J.E. Demuth, W.J. Thompson, N.J. DiNardo, and R. Imbihl, Phys. Rev. Lett. **56**, 1408 (1986).

[14] S.M. Sze, *Physics of Semiconductor Devices*, (J. Wiley, 1981).

[15] M. Lax, Journal of Applied Physics **48**, 3919 (1977).

[16] M.A. Olmstead, N.M. Amer, and S. Kohn, Appl. Phys. A **32**, 141 (1983).

[17] R.J. Hamers, R.M. Tromp, and J.E. Demuth, Phys. Rev. Lett. **56**, 1972 (1986).

[18] F.J. Himpsel and Th. Fauster, J. Vac. Sci. Tech. A **2**, 815 (1984).

Figure Captions

Figure 1. Schematic illustration of surface photovoltage effect, as described in text.

Figure 2. Diagram of optical system. EOM: Electro-optic modulator; PP: Polarizing prism; BS: Beamsplitter; PD: Photodiode.

Figure 3. Tunneling I-V curves measured on clean p-type Si(111)-(7X7) in the absence and presence of optical illumination, stabilization voltage = +1.2 V.

Figure 4. Schematic of the electronics used for photovoltage measurements. Electronics denoted "1" are active during the topography part of the cycle, those denoted "2" are active during the potentiometry part of the cycle.

Figure 5. Atomically-resolved measurements of topography and surface photovoltage on Si(111)-(7X7) surfaces; a) Topographic image, Sample bias = -1.0 Volt; b) Surface photovoltage, average value = -140 mV; c) 3-dimensional representation of topography data; d) 3-dimensional representation of surface photovoltage data; Arrows in panels a and b indicate position of boundary between two (7X7) domains. The laser was blocked at the rightmost portion of the images.

Figure 6. Dependence of surface photovoltage on laser power on a well-ordered region of Si(111)-(7X7). The dashed line is a fit to a function of the form V = A log (1 + B prime P) as described in the text.

Figure 7. Spatially-resolved SPV measurements at ordered and at defected (7X7) locations; a) Topographic image, Sample voltage = +1.0 Volt; b) Spatially-resolved photovoltage image. Average value = -140 mV; c) Surface photovoltage vs. laser intensity at the locations indicated in fig. 5a and 5b., corresponding to ordered (7X7) region and defect.

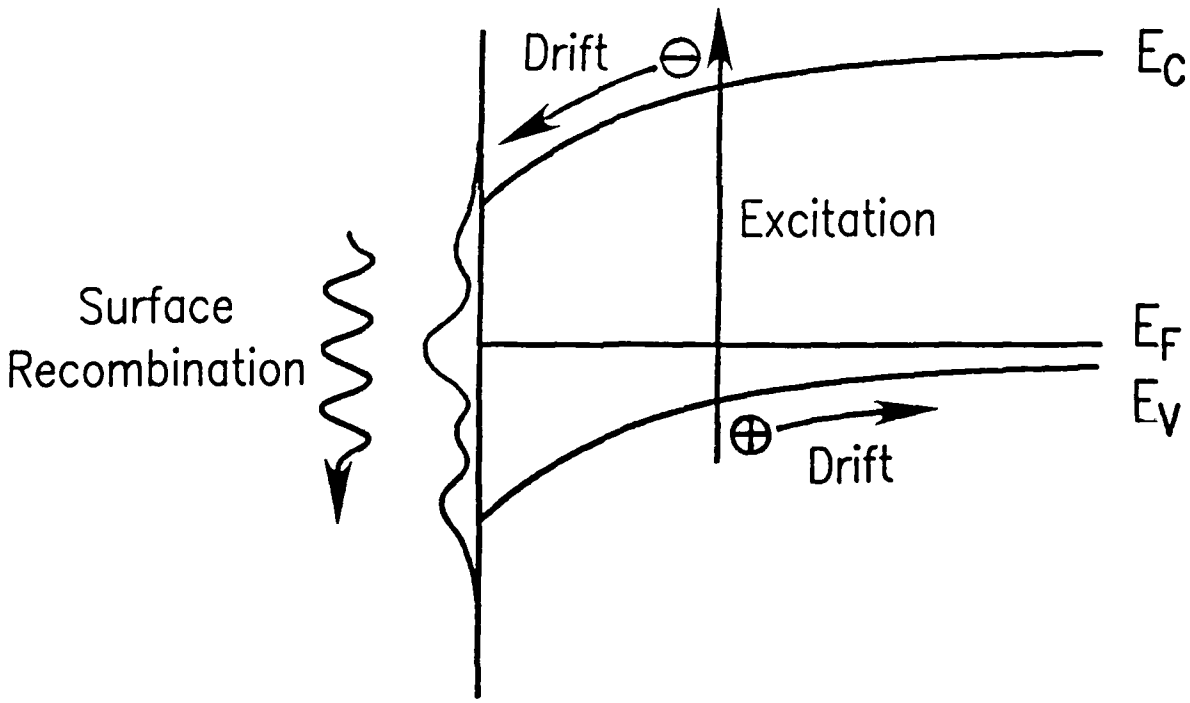

Figure 1
Hamers & Markert

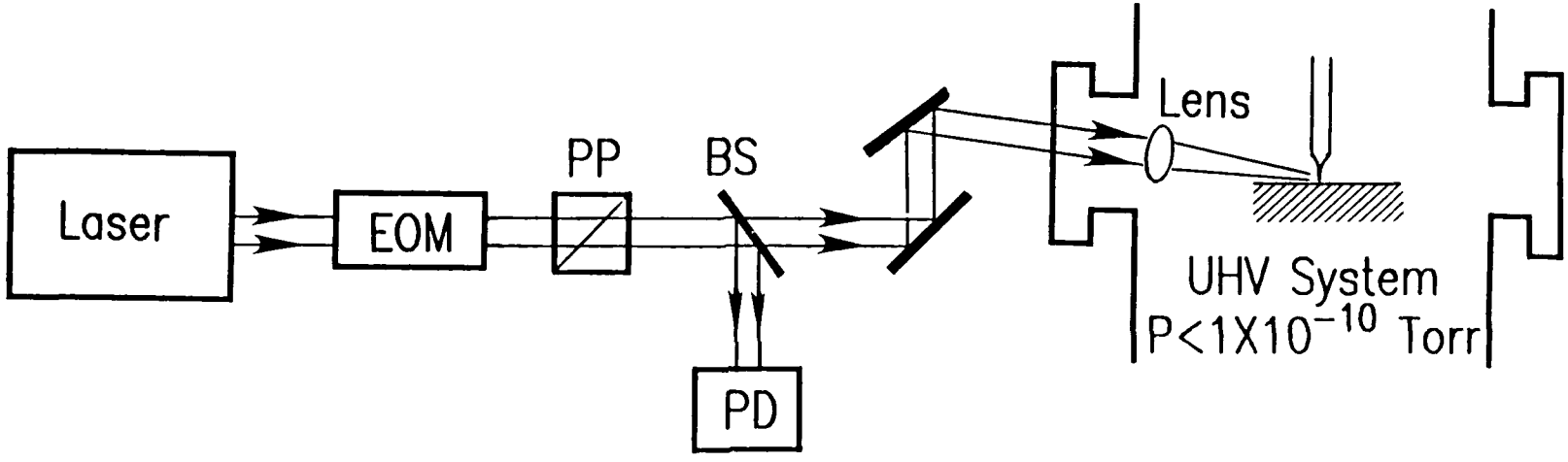

Figure 2
Hamers & Markert

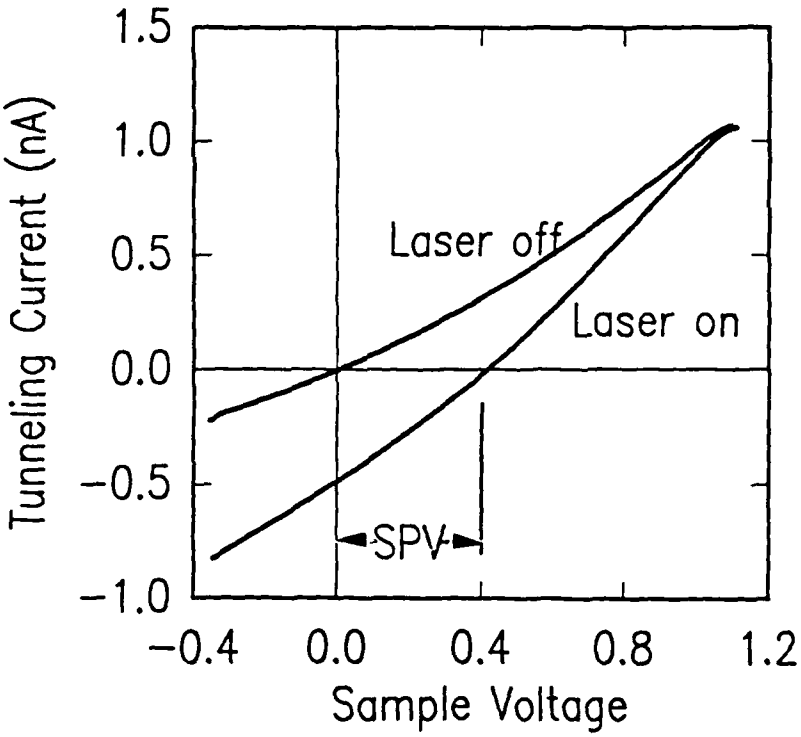
1.5
1.0
0.5
0.0
−0.5
−1.0
Tunneling Current (nA)
Laser off
Laser on
SPV
−0.4
0.0
0.4
0.8
1.2
Sample Voltage

Figure 3

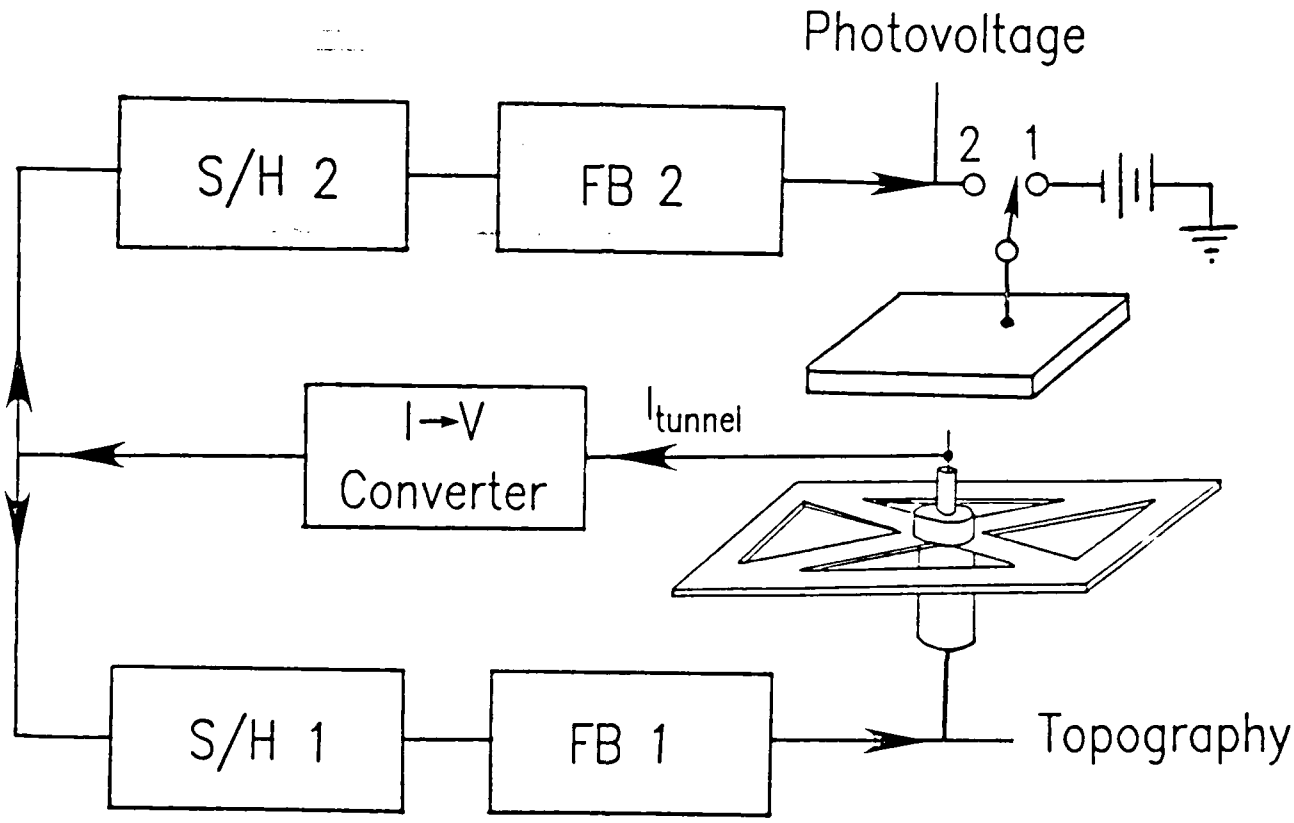

Figure 4
Hamers & Markert

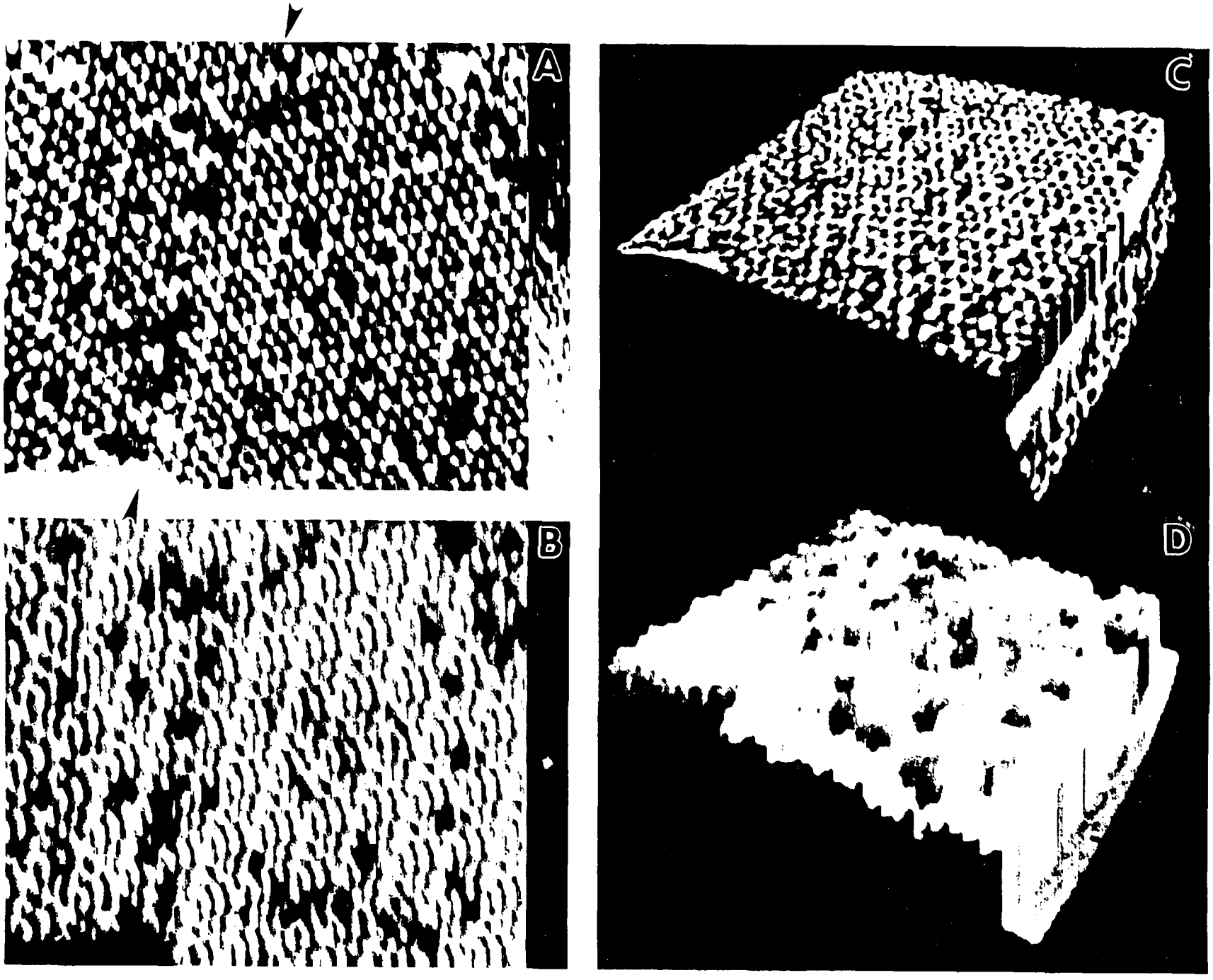

Fig. 5
Hamers & Markert

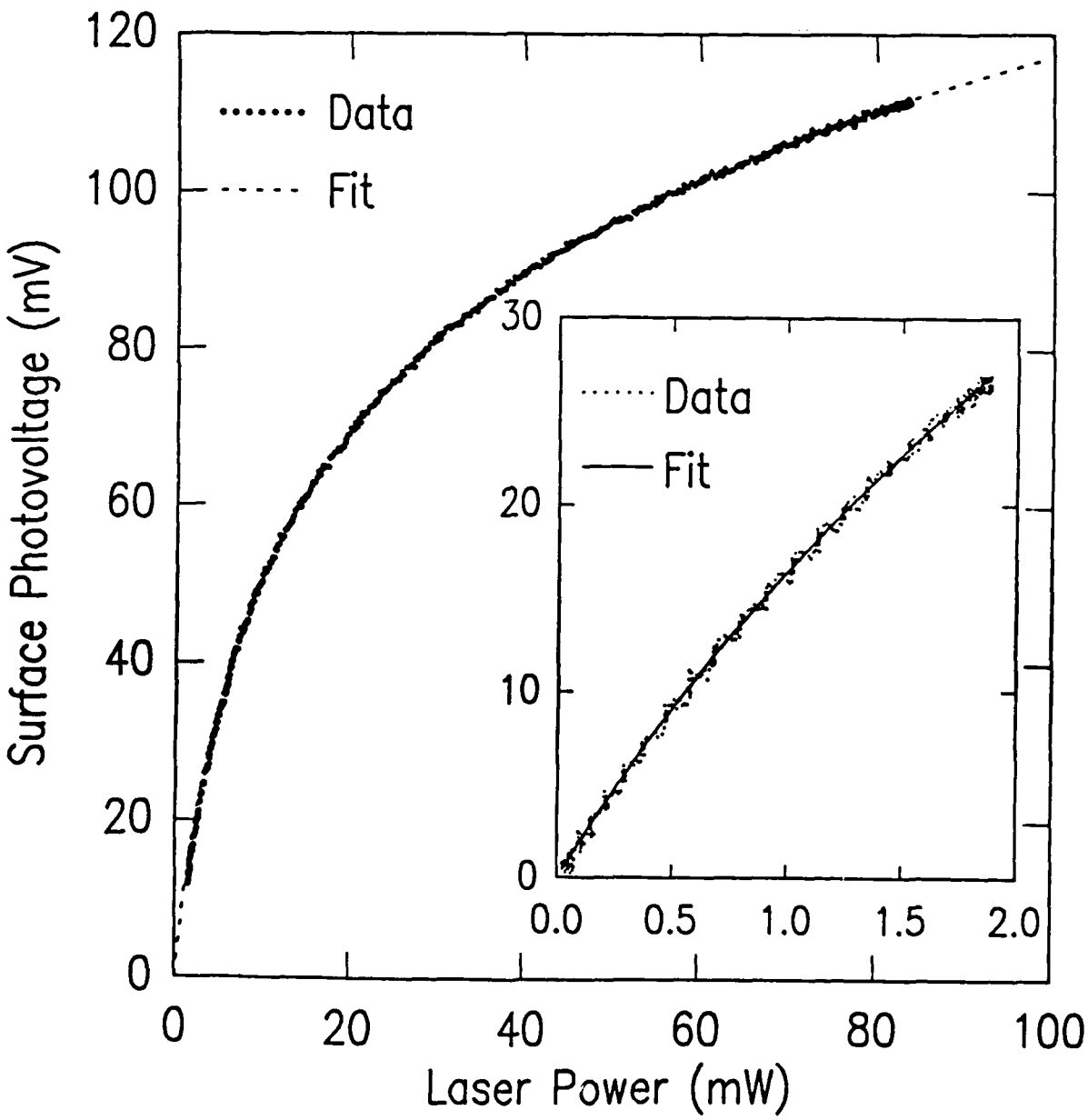

Fig. 6
Hamers & Marker

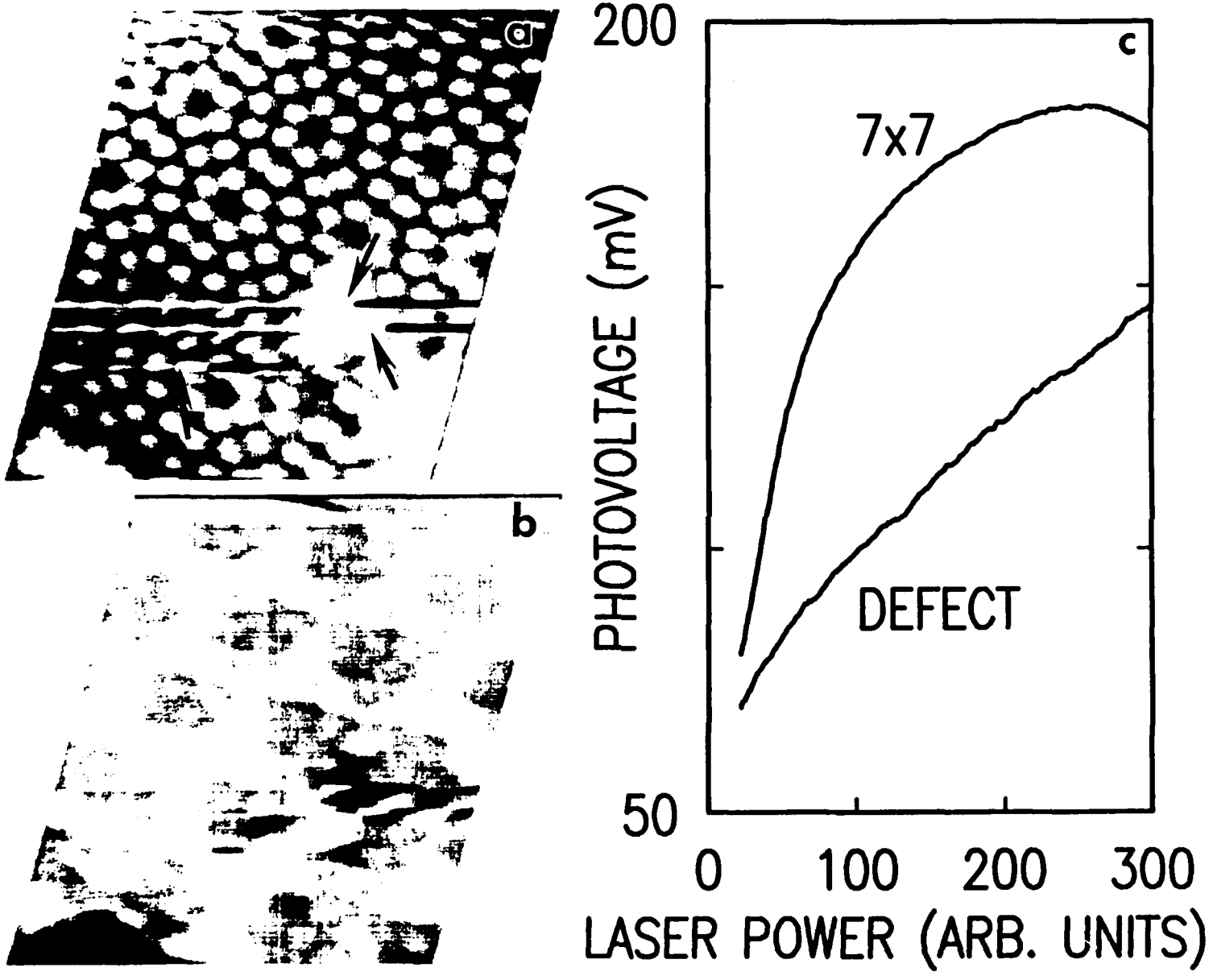

Figure 7
Hamers & Markert